

Universal resilience patterns in complex networks

Jianxi Gao^{1*}, Baruch Barzel^{2*} & Albert-László Barabási^{1,3,4,5}

Resilience, a system's ability to adjust its activity to retain its basic functionality when errors, failures and environmental changes occur, is a defining property of many complex systems¹. Despite widespread consequences for human health², the economy³ and the environment⁴, events leading to loss of resilience—from cascading failures in technological systems⁵ to mass extinctions in ecological networks⁶—are rarely predictable and are often irreversible. These limitations are rooted in a theoretical gap: the current analytical framework of resilience is designed to treat low-dimensional models with a few interacting components⁷, and is unsuitable for multi-dimensional systems consisting of a large number of components that interact through a complex network. Here we bridge this theoretical gap by developing a set of analytical tools with which to identify the natural control and state parameters of a multi-dimensional complex system, helping us derive effective one-dimensional dynamics that accurately predict the system's resilience. The proposed analytical framework allows us systematically to separate the roles of the system's dynamics and topology, collapsing the behaviour of different networks onto a single universal resilience function. The analytical results unveil the network characteristics that can enhance or diminish resilience, offering ways to prevent the collapse of ecological, biological or economic systems, and guiding the design of technological systems resilient to both internal failures and environmental changes.

The traditional mathematical treatment of resilience used from ecology⁴ to engineering⁵ approximates the behaviour of a complex system with a one-dimensional (1D) nonlinear dynamic equation

$$\frac{dx}{dt} = f(\beta, x) \quad (1)$$

The functional form of $f(\beta, x)$ represents the system's dynamics, and the parameter β captures the changing environmental conditions. The system is assumed to be in one of the stable fixed points, x_0 , of equation (1), extracted from⁵

$$f(\beta, x_0) = 0 \quad (2)$$

$$\left. \frac{\partial f}{\partial x} \right|_{x=x_0} < 0 \quad x(\beta) = x_0 \quad (3)$$

where equation (2) provides the system's steady state and equation (3) guarantees its linear stability. The solution of equations (2) and (3) provides the resilience function $x(\beta)$, which represents the possible states of the system as a function of β (Fig. 1a–c). The shape of this function is uniquely determined by the functional form of $f(\beta, x)$. In contrast, the momentary state of the system is determined by the tunable parameter β . At some critical point β_c the resilience function may feature a bifurcation (Fig. 1a) or become non-analytic (Fig. 1b, c), indicating that

the system loses its resilience by undergoing a sudden transition to a different^{8,9}, often undesirable, fixed point of equation (1).

Although it is conceptually powerful, this analytic framework does not account for the exceptionally large number of variables that in reality control the state of a complex system. Indeed, real systems are composed of numerous components linked via a complex set of weighted, often directed, interactions^{10,11}, and controlled by not one microscopic parameter, but by a large family of parameters, such as the weights of all interactions. Hence, instead of a 1D function $f(\beta, x)$, characterized by a single parameter β , their state should be described by a network of coupled nonlinear equations that capture the interactions between the system's many components, and account for the complex interplay between the system's dynamics and changes in the underlying network topology^{6,12}. The resulting resilience function is therefore a multi-dimensional manifold over the complex parameter space characterizing the system (Fig. 1d–f), which, using the current tools, cannot be treated analytically. Here we overcome these longstanding limitations by developing a general network-based theoretical framework that allows us to explore and predict the multiple roots and dimensions of resilience, exposing crucial determinants of resilience loss in complex natural and man-made systems.

Consider a system consisting of N components (nodes) whose activities $\mathbf{x} = (x_1, \dots, x_N)^\top$ follow the coupled nonlinear equations^{12,13}

$$\frac{dx_i}{dt} = F(x_i) + \sum_{j=1}^N A_{ij}G(x_i, x_j) \quad (4)$$

self dynamics

The first term on the right-hand side of equation (4) describes the self-dynamics of each component, while the second term describes the interactions between component i and its interacting partners. The nonlinear functions $F(x_i)$ and $G(x_i, x_j)$ represent the dynamical laws that govern the system's components, while the weighted connectivity matrix $A_{ij} > 0$ captures the positive interactions between the nodes. With an appropriate choice of $F(x_i)$ and $G(x_i, x_j)$, equation (4) is used to model numerous systems known for their resilience, ranging from cellular¹⁴ to ecological^{15,16} and social systems¹⁷.

In analogy with the 1D system of equation (1), a transition from a desired to an undesired stable fixed point captures the loss of resilience in the multi-dimensional system of equation (4). The key difference is that in equation (4) resilience loss can be induced by changes in any of the N^2 parameters of the weighted network A_{ij} , each change capturing a different kind of perturbation (Fig. 1g). For instance, the extinction/introduction of species in an ecological system may correspond to the removal/addition of one or several nodes^{7,18}. Alternatively, the loss of an enzyme catalysing a reaction in a metabolic network¹⁹ may correspond to link removal. Finally, global environmental changes, such as increases in ocean acidity or global warming²⁰, may correspond to global shifts in the weights of A_{ij} .

We illustrate the challenges such multi-dimensional systems offer by exploring the mutualistic interactions among species in an ecological

¹Center for Complex Network Research, Department of Physics, Northeastern University, Boston, Massachusetts 02115, USA. ²Department of Mathematics, Bar-Ilan University, Ramat-Gan 52900, Israel. ³Center for Cancer Systems Biology, Dana-Farber Cancer Institute, Harvard University, Boston, Massachusetts 02215, USA. ⁴Department of Medicine, Brigham and Women's Hospital, Harvard Medical School, Boston, Massachusetts 02115, USA. ⁵Center for Network Science, Central European University, Budapest 1051, Hungary.

*These authors contributed equally to this work.

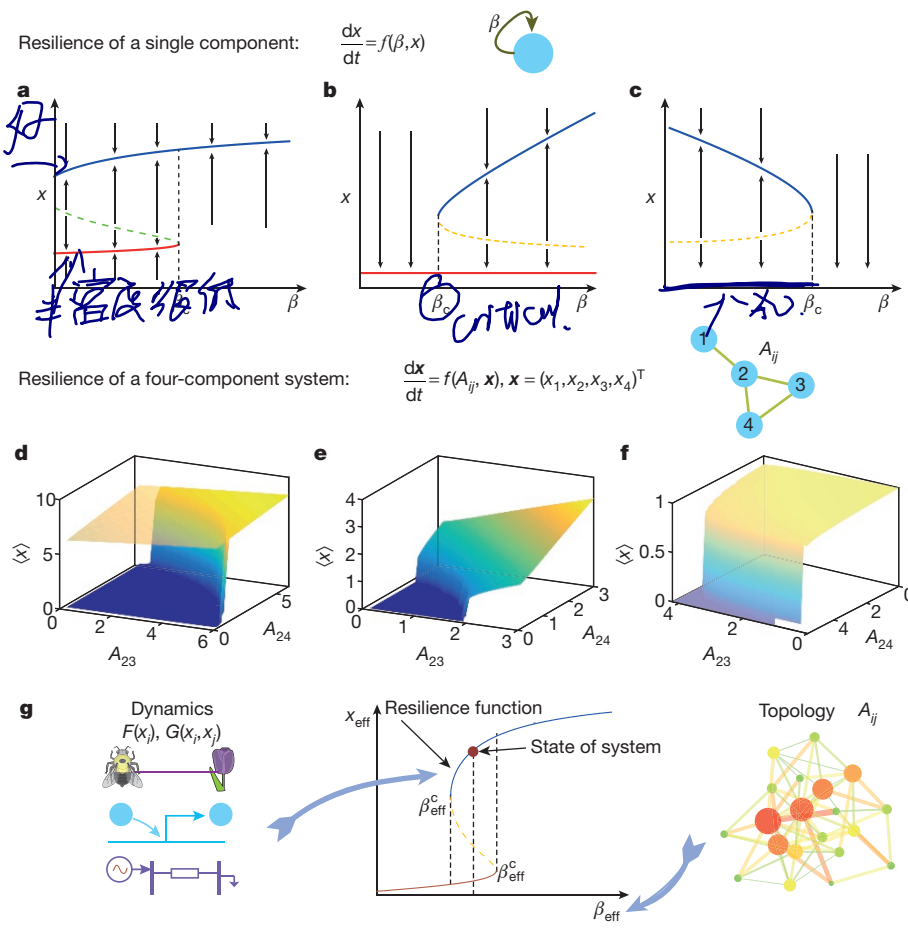


Figure 1 | Network resilience. **a–c**, In 1D systems resilience is captured by the resilience function $x(\beta)$, which describes the state(s) of the system as a function of the tunable parameter β . We illustrate three typical examples. **a**, The bifurcating resilience function. The system exhibits a single stable fixed point for $\beta > \beta_c$ (blue) and two (or more) stable fixed points, a desired (blue) and an undesired (red) for $\beta < \beta_c$. **b**, Resilience function with a first-order transition from the desired (blue) state to the undesired (red) state. **c**, Resilience function with a stable solution for $\beta < \beta_c$ and no solution above β_c , resulting in an uncontrolled divergent or chaotic behaviour. **d–f**, In a multi-dimensional system, the single parameter β is replaced by the complex weighted network A_{ij} , whose characteristics depend on both environmental conditions and the specific pairwise interaction strengths. Consequently, the resilience function, now capturing the behaviour of the vector state $x(A_{ij})$, is a multi-dimensional manifold, prohibiting analytical treatment. The 3D plots show the resilience plane for a four-node system, displaying $x(A_{23}, A_{24})$ for fixed A_{12} and A_{34} . The full description of an N -dimensional system requires an N^2 -dimensional plane, tracking the state of the system as a function of all A_{ij} . **g**, After applying our formalism, the multi-dimensional manifold shown in **d–f** collapses into a 1D resilience function in β -space (blue and red solid lines). The structure of this function, and hence its critical points β_{eff}^c (dashed lines) is fully determined by the system's dynamics $F(x_i)$ and $G(x_i, x_j)$: ecological, regulatory power transmission and so on (left). The network topology A_{ij} (right) determines β_{eff} through equation (8), and hence the specific state of the system (brown dot) along the resilience function.

network. Here equation (4) tracks the abundance $x_i(t)$ of species i , following¹⁶

$$\frac{dx_i}{dt} = B_i + x_i \left(1 - \frac{x_i}{K_i}\right) \left(\frac{x_i}{C_i} - 1\right) + \sum_{j=1}^N A_{ij} \frac{x_i x_j}{D_i + E_i x_i + H_j x_j} \quad (5)$$

The first term on the right hand side of equation (5) accounts for the incoming migration of i at a rate B_i from neighbouring ecosystems. The second term describes logistic growth with the system carrying capacity²¹ K_i , and the Allee effect, according to which for low abundance ($x_i < C_i$) the system features negative growth²². The third term describes mutualistic interactions, captured by a response function that saturates for large x_i or x_j , indicating that j 's positive contribution to x_i is bounded. To construct A_{ij} we used symbiotic interactions, such as plant–pollinator relationships, collected for seven ecological systems²³ (Supplementary Table 1), describing networks ranging from $N = 10$ to $N = 1,429$ nodes (Fig. 2a, b). We numerically solved equation (5), and tested its resilience under three realistic perturbations (Fig. 2c): first, we randomly removed a fraction f_n of nodes, capturing plant extinctions; second, we removed a random fraction f_p of pollinators, thus perturbing the mutualistic link weights; and finally, we randomly rescaled all the weights A_{ij} , reducing their strength on average by a fraction f_w to mimic global environmental changes.

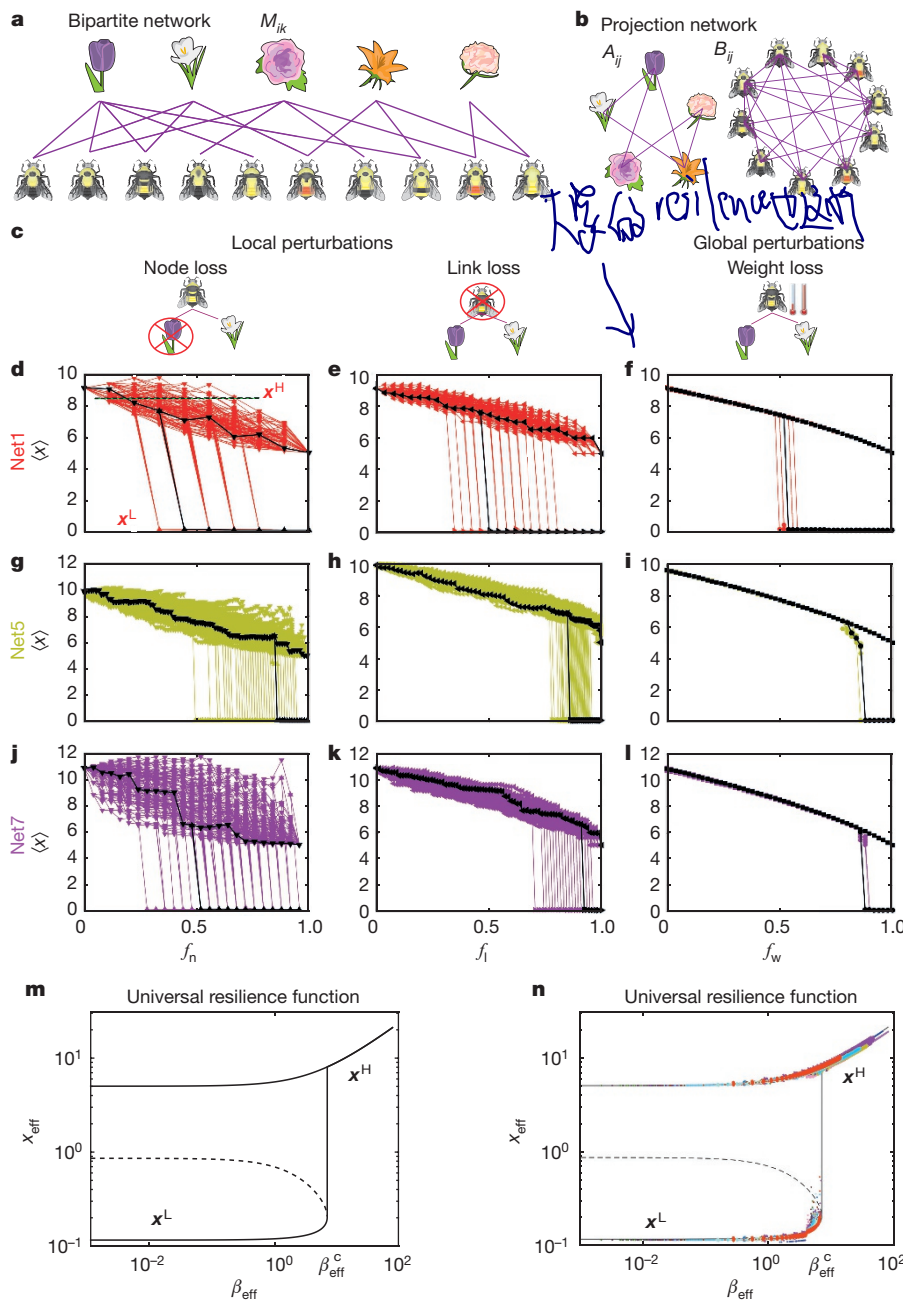
We find that for small perturbations the system maintains its resilience: its only stable fixed point is x^H , in which the average abundance $\langle x \rangle$ is high. However, when the perturbation exceeds a certain threshold a bifurcation occurs, resulting in two stable fixed points: the desired x^H and an undesired low-abundance state x^L (Fig. 2d). Under these conditions the system loses its resilience, potentially transitioning to the undesired x^L . The precise bifurcation point marking this loss of resilience is, however, highly unpredictable. For instance,

Net1 displays a different resilience pattern for node removal (Fig. 2d), link removal (Fig. 2e) or global weight changes (Fig. 2f), indicating that different forms of perturbations lead to different outcomes within the same system. Such diversity is also observed for similar perturbations across different systems. For example, while we need to remove at least 35% of the pollinators for Net1 to lose its resilience (Fig. 2e), Net5 remains resilient even after 80% of its pollinators are deleted (Fig. 2h). Finally, even the sequence in which the perturbation is applied makes an important difference: Net1 can lose its resilience anywhere between the removal of 30% to 70% of its nodes (Fig. 2d), depending on the specific trial.

Altogether, we analysed fourteen experimentally mapped networks (Supplementary Table 1), finding that the resilience transition depends on the network topology, the form and the nature of the perturbation applied and the specific realization (Fig. 2d–l, and Supplementary Figs 2–4), exposing severe limits to our ability to predict the network resilience. We now show that this seemingly unpredictable behaviour can be systematically treated by focusing on the system's natural state and control variables. In a network environment, the state of each node is affected by the state of its immediate neighbours. Therefore, we characterize the effective state of the system using the average nearest-neighbour activity

$$x_{eff} = \frac{\mathbf{I}^\top A \mathbf{x}}{\mathbf{I}^\top A \mathbf{I}} = \frac{\langle s^{out} x \rangle}{\langle s \rangle} \quad (6)$$

where $s^{out} = (s_1^{out}, \dots, s_N^{out})^\top$ is the vector of outgoing weighted degrees and $s^{in} = (s_1^{in}, \dots, s_N^{in})^\top$ is the vector of incoming weighted degrees, $\langle s^{out} x \rangle = (1/N) \sum_{i=1}^N s_i^{out} x_i$, $\langle s \rangle = \langle s^{in} \rangle = \langle s^{out} \rangle$ is the average weighted degree, and \mathbf{I} is the unit vector $\mathbf{I} = (1, \dots, 1)^\top$. As we show in Supplementary Information section I, if A_{ij} has not much degree correlation, the variable x_{eff} in equation (6) allows us to reduce the

**Figure 2 | Resilience in ecological networks.**

a, The bipartite network M_{ik} consists of nodes representing symbiotically connected species, such as plants and pollinators or fish and anemone. **b**, From M_{ik} we construct two mutualistic networks (Supplementary Information section II.B) by linking pairs of plants that share mutual pollinators (A_{ij}), or pollinators that share mutual plants (B_{ij}). **c**, We tested the resilience of fourteen mutualistic networks (equation (5); $B_i = B = 0.1$, $C_i = C = 1$, $K_i = K = 5$, $D_i = D = 5$, $E_i = E = 0.9$ and $H_j = H = 0.1$) against: (1) extinction of a fraction f_n of plants; (2) extinction of a fraction f_i of pollinators, impacting the relevant plant link weights; (3) decreasing all weights on average to a fraction f_w of their original value, simulating a global change in the environmental conditions, for example, varying temperature. **d**, The average abundance of fish in Net1 versus f_n across 100 realizations (we highlight one of these realizations in black). At a critical fraction f_n the system undergoes a bifurcation, where in addition to the high-abundance state (x^H) an undesired low-abundance state emerges (x^L). However, owing to the multi-dimensionality of A_{ij} , each realization is microscopically distinct, and as a result the bifurcation point is unpredictable, ranging from $f_n = 0.3$ to $f_n = 0.7$ across different realizations. **e**, **f**, Similar diversity characterizes the system's response to link perturbation f_i (**e**) and global perturbations f_w (**f**). **g–l**, The difficulty in predictability is also observed in the larger networks Net5 and Net7. Additional results appear in Supplementary Figs 2–4. **m**, Our formalism predicts that in β -space the resilience function takes a universal form, similar to that shown in Fig. 1a, with bifurcation at $\beta_{\text{eff}}^c = 6.97$, independent of A_{ij} . **n**, All data in **d–l** and in Supplementary Figs 2–4, comprising 28 highly diverse networks, collapses onto the universal resilience function predicted in **m**, indicating that regardless of the network structure and the form of perturbation, the state of the system is fully determined by β_{eff} (equation (8)).

multi-dimensional equation (4) to an effective 1D equation, written in terms of x_{eff}

$$(7)$$

where

$$(8)$$

averages over the product of the outgoing and incoming degrees of all nodes. This reduction maps the multi-dimensional complex system (4) into an effective 1D equation of the form of equation (1), where

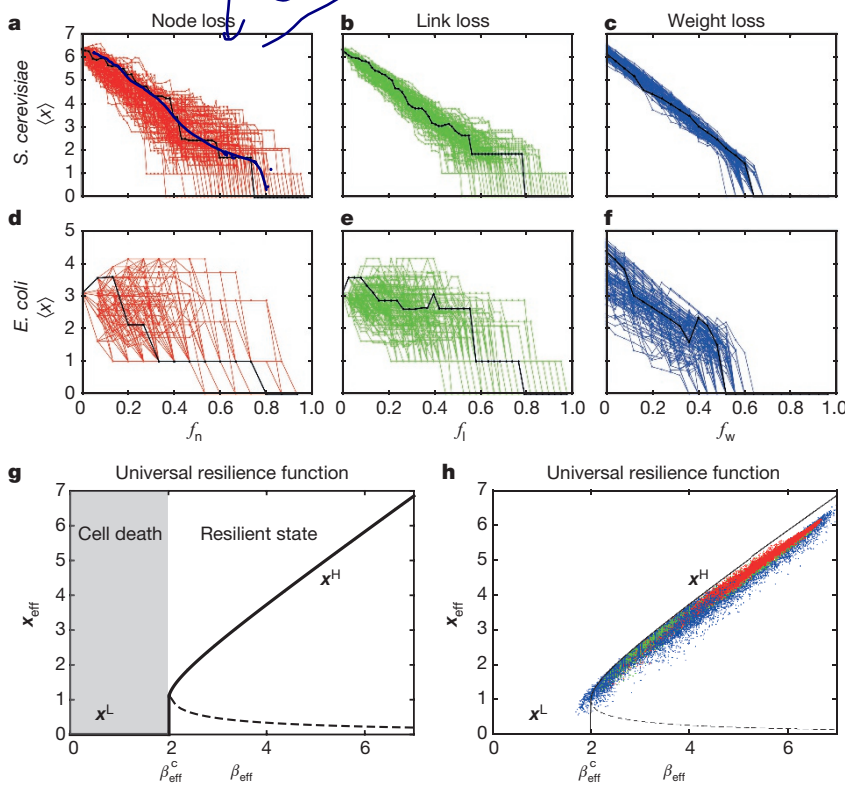
$$(9)$$

We predict, therefore, that the N^2 parameters of the microscopic description A_{ij} collapse into a single macroscopic resilience parameter β_{eff} (see equation (8)), so that regardless of the microscopic details

of the perturbation (node/link removal, weight reduction or any combination thereof), its impact on the state of the system is fully accounted for by the corresponding changes in β_{eff} . This implies that the rather diverse and unpredictable behaviours observed in Fig. 2 are, in fact, drawn from a single universal resilience function, independent of the network topology A_{ij} , and uniquely determined by the system's dynamics $F(x_i)$ and $G(x_i, x_j)$. The network A_{ij} , which is fully condensed into the single macroscopic parameter β_{eff} , determines only the specific state of the system along this function. Such mapping of equation (4) to the 1D equation (7) allows us to take advantage of the theoretical tools developed for low-dimensional systems and apply them to a broad range of complex systems.

To illustrate the power of our formalism we apply it to the mutualistic networks of Fig. 2. Reducing the multi-dimensional equation (5) to the form of equation (9) we arrive at the 1D equation (Supplementary Information section II)

$$(10)$$

**Figure 3 | Resilience in gene regulatory networks.**

We ran Michaelis–Menten dynamics (equation (11)) on the transcription regulatory networks of *S. cerevisiae*²⁴ and *E. coli*²⁵ (Supplementary Table 2) to model the dynamics of genetic regulation, providing the average activity $\langle x \rangle$ of all genes. **a**, By removing a sufficiently high fraction f_n of nodes the system undergoes a transition from $x^H > 0$ (alive) to $x^L = 0$ (cell death). The transition point occurs at a different value of f_n in each realization. **b, c**, Similar results are found for link perturbations and global weight changes. **d–f**, The same diversity is observed for the *E. coli* network as well. **g**, Our formalism predicts that the behaviour of gene regulation is captured by a universal resilience function of the form of Fig. 1b, with a single first-order transition at $\beta_{\text{eff}}^c = 2$. This function is determined by the regulatory dynamics of equation (11), and is independent of the network structure or the nature of its perturbations. **h**, The results of a–f shown in β -space. Regardless of the system's microscopic details, all observed data points, taken from *S. cerevisiae* or *E. coli*, induced by node perturbations (red), link perturbations (green) or weight changes (blue), collapse onto the same curve, well approximated by the analytically predicted universal resilience function (solid line).

Using equations (2) and (3), equation (10) predicts a bifurcating resilience function of the form of Fig. 1a, and a transition from a resilient state with a single stable fixed point, x^H , to a non-resilient state in which both x^H and x^L are stable. The critical point of this bifurcation is predicted to be $\beta_{\text{eff}}^c = 6.97$, a value fully determined by the dynamics, independent of the network topology A_{ij} (Fig. 2m and Supplementary Information section II).

Our formalism predicts that the diversity observed in Fig. 2d–l and in Supplementary Figs 2–4, is, in fact, driven by the universal curve of Fig. 2m. This universality can be exposed by transitioning to the natural parameter space of x_{eff} (see equation (6)) and β_{eff} (see equation (8)). Hence we re-plotted all the data of Fig. 2d–l (and Supplementary Figs 2–4, 28 diverse networks in total), in this effective β -space, finding that, as predicted, all data points collapse into a single universal curve, regardless of the size and the topology of the specific ecological network or the nature of the applied perturbation (Fig. 2n). This collapse indicates that our analytically predicted resilience function exposes a universality sustained across networks of different size, density, degree and weight distributions. Additional extensive testing of this universality appears in Supplementary Information section V.

In summary, the resilience pattern of a complex system is effectively unpredictable in the natural (x, A_{ij}) state parameter space. Once, however, we map the system into β -space we can accurately predict the system's response to diverse perturbations and correctly identify the critical points where the system loses its resilience.

Next we explore the resilience of gene regulatory networks governed by the Michaelis–Menten equation¹⁴

$$\frac{dx_i}{dt} = -Bx_i^f + \sum_{j=1}^N A_{ij} \frac{x_j^h}{x_j^h + 1} \quad (11)$$

The first term on the right-hand side of equation (11) describes degradation ($f=1$) or dimerization ($f=2$); the second term captures genetic activation, where the Hill coefficient h describes the level of cooperation in gene regulation¹⁴. Applying this model with $B=1$, $f=1$ and $h=2$ to the transcription networks of *Saccharomyces cerevisiae*²⁴ and *Escherichia coli*²⁵, we find that under sufficiently large perturbations

the cell undergoes a transition from a resilient state ($\langle x \rangle > 0$) to cell death ($\langle x \rangle = 0$, Fig. 3a–f). Once again, resilience loss strongly depends on the nature of the perturbation (gene knockout, suppression of regulatory interactions, environmental change), as well as on the differences between the wiring diagrams of *S. cerevisiae* versus *E. coli* (Supplementary Table 2). Rewriting equation (11) in the reduced form of equation (7), we find that regulatory dynamics follow the universal resilience function shown in Fig. 1b, featuring a single first-order transition from the active state to cell death at (Supplementary Information section III)

$$\beta_{\text{eff}}^c = \frac{Bh}{h-f} \left(\frac{h-f}{f} \right)^{\frac{f}{h}} \quad (12)$$

Indeed, in β -space, all trajectories of Fig. 3a–f collapse onto the analytically derived resilience function, as predicted by our formalism (Fig. 3h). In Supplementary Information section IV we develop another application area, demonstrating how to apply our formalism to predict the resilience of energy supply in the power grid.

Although the resilience function is uniquely determined by the dynamical functions $F(x_i)$ and $G(x_i, x_j)$, the actual position of the system along this curve, capturing its momentary state, is determined by the weighted network topology A_{ij} , as expressed through β_{eff} in equation (8). This prompts us to ask what aspects of the network topology determine a system's resilience. We therefore rewrite β_{eff} as

$$\beta_{\text{eff}} = \langle s \rangle + \mathcal{SH} \quad (13)$$

where $\langle s \rangle$, \mathcal{S} and \mathcal{H} represent three characteristics of A_{ij} . The dependence on the network density $\langle s \rangle$ indicates that denser networks have a larger β_{eff} (Fig. 4a). The heterogeneity in the weighted degrees s^{in} and s^{out} is captured by $\mathcal{H} = \sigma_{\text{in}}\sigma_{\text{out}}/\langle s \rangle$, where σ_{in}^2 and σ_{out}^2 are the variance of the marginal probability density functions $P(s^{\text{in}})$ and $P(s^{\text{out}})$ respectively (Fig. 4b). Finally, the symmetry between s^{in} and s^{out} is captured by $\mathcal{S} = (\langle s^{\text{in}}s^{\text{out}} \rangle - \langle s^{\text{in}} \rangle \langle s^{\text{out}} \rangle)/(\sigma_{\text{in}}\sigma_{\text{out}})$, the in–out weighted-degree correlation coefficient. This term, $-1 \leq \mathcal{S} \leq 1$, is positive when nodes

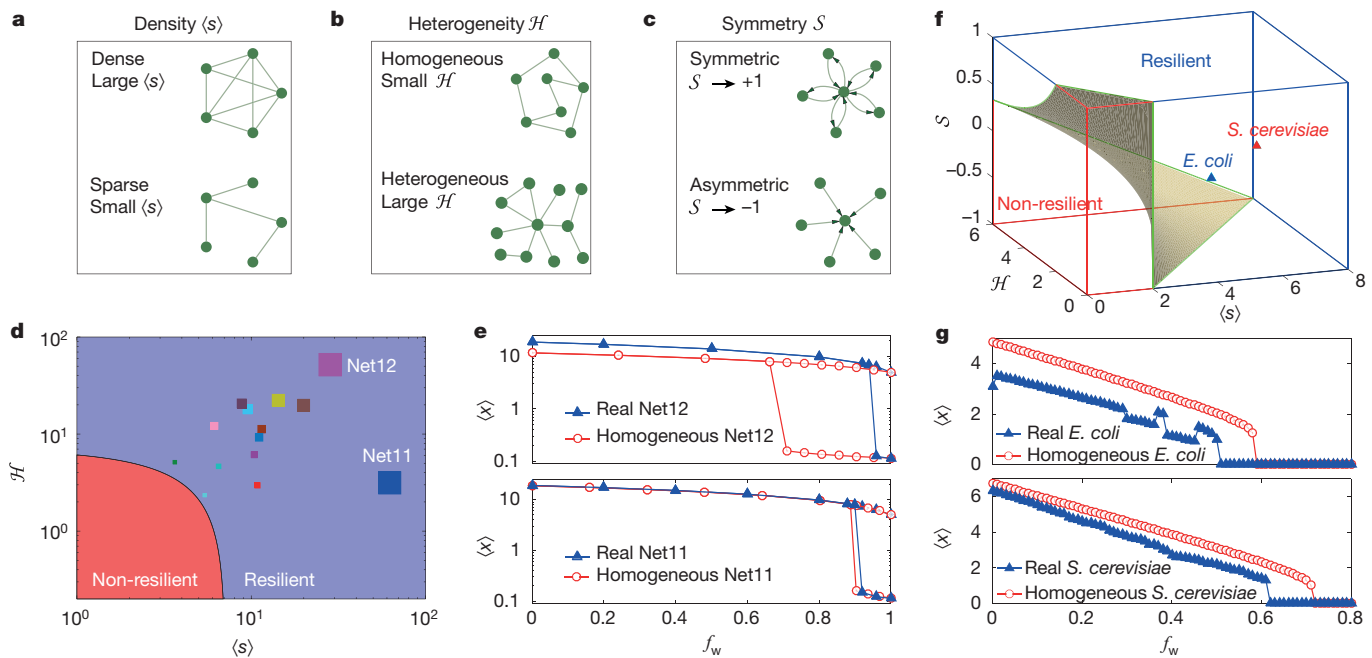


Figure 4 | The impact of A_{ij} on resilience. The topological characteristics that affect a system's resilience through β_{eff} (equation (13)) are: **a**, the network density $\langle s \rangle$; **b**, the heterogeneity in degrees or link weights H ; and **c**, the symmetry S , capturing the correlations between a node's in and out degrees. **d**, Phase diagram for mutualistic dynamics in the $\langle s \rangle$ - H plane. In the resilient phase, the system has a single stable fixed point x^L ; in the non-resilient phase the undesired x^U is also stable. For this dynamics the greater β_{eff} is (square size) the deeper the system is in the resilient phase. **e**, The average state of the system $\langle x \rangle$ versus the average reduction in the link weights. For Net12, the most heterogeneous of the fourteen mutualistic networks, we observe an extreme degree of resilience, avoiding collapse up to $f_w = 97\%$ (blue triangles). A homogeneous network, with the

with large s_i^{in} tend also to have a large s_i^{out} . An undirected network $A_{ij} = A_{ji}$ is a perfectly symmetric network, as $s_i^{\text{in}} = s_i^{\text{out}}$, hence $S = 1$; an asymmetric network is one where nodes with a large in-degree tend to have a small out-degree, in which case $S < 0$, tending towards -1 (Fig. 4c).

Equation (13) helps us to identify the network characteristics that can enhance or weaken a system's resilience. Consider for example the resilience of the ecosystem described in equation (5). The structure of the resilience function (Fig. 2m) indicates that the greater is β_{eff} , the more resilient is the system, enduring larger perturbations before reaching the bifurcation at β_{eff}^c and risking a transition to the undesired x^U . Since mutualistic networks are symmetric we have $S=1$ and $H = \sigma_{\text{in}}/\sigma_{\text{out}}/\langle s \rangle \equiv \sigma^2/\langle s \rangle$, obtaining $\beta_{\text{eff}} = \langle s \rangle + \sigma^2/\langle s \rangle$. Hence, equation (13) increases both with density $\langle s \rangle$ and with heterogeneity H giving rise to a 2D phase space: a resilient phase above the phase boundary $\langle s \rangle + H = \beta_{\text{eff}}^c$, and a non-resilient phase below it. In Fig. 4d we show all fourteen mutualistic networks and their location on the $\langle s \rangle$ - H phase diagram, characterizing the source of each network's resilience. For instance, Net11 and Net12 have comparable β_{eff} values and hence comparable levels of resilience, indicating that both can withstand comparable levels of perturbation before crossing the bifurcation at β_{eff}^c . However, Fig. 4d shows that while the source of Net11's resilience is its high density $\langle s \rangle$, the source of Net12's resilience is its high heterogeneity H . To test this we constructed two homogeneous networks with the same densities as Net11 and Net12, but with $H=0$. As expected for Net12, reducing heterogeneity greatly decreased resilience (by $\sim 30\%$), while for Net11, whose source of resilience is density rather than heterogeneity, eliminating H had only a negligible impact (Fig. 4d, e).

In regulatory dynamics the phase diagram has two domains, corresponding to an active phase and cell death. Here resilience increases

same density and $H=0$ loses resilience at $f_w = 66\%$ (red circles); hence H is the source of Net12's exceptional resilience. As indicated in d, Net11's resilience is rooted in its high density $\langle s \rangle$. Indeed, we find that for Net11, both the original (blue triangles) and the homogeneous (red circles) networks feature comparable levels of resilience, indicating that H has a marginal contribution. **f**, The phase diagram for directed transcription regulatory networks is 3D— $\langle s \rangle$, H and S —with the first-order transition from a living cell to cell death occurring at $\langle s \rangle + SH = 2$. The position of the *S. cerevisiae* and the *E. coli* networks is also shown (triangles). **g**, For both organisms $S < 0$, and hence heterogeneity decreases their resilience: indeed, the homogeneous networks (red circles) withstand larger perturbations than the original networks (blue triangles).

with β_{eff} , as the larger is β_{eff} , the deeper is the system into the active state, and farther from the critical transition at β_{eff}^c (equation (12)). Since A_{ij} is directed, H can both increase or decrease β_{eff} , depending on the symmetry S in equation (13). Consequently, resilience is governed by three topological characteristics, where dense, symmetric and heterogeneous networks are most resilient (large β_{eff}), and sparse, antisymmetric and heterogeneous networks are least resilient (small β_{eff}). The phase diagram in the $\langle s \rangle$ - H - S space is shown in Fig. 4f, and the transition between states occurs along the plane $\langle s \rangle + SH = \beta_{\text{eff}}^c$. For the two regulatory networks we measured $S = -0.083$ (for *S. cerevisiae*) and $S = -0.2464$ (for *E. coli*), both negative. Hence here H has a negative contribution to resilience and a homogeneous network with $H=0$ would, in fact, be more resilient. To test this prediction we compared the resilience function of the empirical networks (*E. coli* and *S. cerevisiae*) with that of the equivalent homogeneous networks in which $\langle s \rangle$ is preserved and $H=0$ (Fig. 4g). Indeed, we find that eliminating heterogeneity increases the system's resilience.

Complex systems are characterized by an inherently multi-dimensional parameter space, giving rise to diverse and unpredictable behaviour. Here, by reverting to the natural parameter space (β -space) we exposed the hidden universal patterns of network resilience. The origin of this universality is in the separation of the system's dynamics and topology. Indeed, in most systems the intrinsic behaviour of the components and the nature of the interactions between them are invariant to perturbations¹³. Perturbations only affect the structure of the network, A_{ij} , determining who interacts with whom and how strongly. Our formalism reduces A_{ij} into an effective 1D system, showing that regardless of the specific topology and weights, or the form of perturbation, the patterns of resilience depend only on the system's intrinsic dynamics. The role of the network topology is fully captured by the

1D β_{eff} , predicting that density, heterogeneity and symmetry are the three key structural factors affecting a system's resilience. They do not alter the critical points, but instead push a system far away from these critical points, helping the system to sustain large perturbations. This separation of structure and dynamics provides us with testable predictions for the system's response to different perturbations. It also suggests potential intervention strategies to avoid the loss of resilience^{26–28}, or design principles for optimal²⁹ resilient systems that can successfully cope with perturbations³⁰.

Received 13 July; accepted 14 December 2015.

1. Cohen, R., Erez, K., Ben-Avraham, D. & Havlin, S. Resilience of the internet to random breakdown. *Phys. Rev. Lett.* **85**, 4626–4628 (2000).
2. Venegas, J. G. et al. Self-organized patchiness in asthma as a prelude to catastrophic shifts. *Nature* **434**, 777–782 (2005).
3. Perrings, C. Resilience in the dynamics of economy-environment systems. *Environ. Resour. Econ.* **11**, 503–520 (1998).
4. May, R. M. Thresholds and breakpoints in ecosystems with a multiplicity of stable states. *Nature* **269**, 471–477 (1977).
5. Lyapunov, A. M. The general problem of the stability of motion. *Int. J. Control.* **55**, 531–534 (1992).
6. Barzel, B. & Biham, O. Quantifying the connectivity of a network: the network correlation function method. *Phys. Rev. E* **80**, 046104 (2009).
7. Sole, R. V. & Montoya, M. Complexity and fragility in ecological networks. *Proc. R. Soc. Lond. B* **268**, 2039–2045 (2001).
8. May, R. M., Levin, S. A. & Sugihara, G. Complex systems: Ecology for bankers. *Nature* **451**, 893–895 (2008).
9. Scheffer, M. et al. Anticipating critical transitions. *Science* **338**, 344–348 (2012).
10. Albert, R. & Barabási, A.-L. Statistical mechanics of complex networks. *Rev. Mod. Phys.* **74**, 47–97 (2002).
11. Ben-Naim, E., Frauenfelder, H. & Toroczkai, Z. *Complex Networks* Vol. 650 (Springer Science & Business Media, 2004).
12. Barzel, B. & Barabási, A.-L. Universality in network dynamics. *Nature Phys.* **9**, 673–681 (2013).
13. Barzel, B., Liu, Y.-Y. & Barabási, A.-L. Constructing minimal models for complex system dynamics. *Nature Commun.* **6**, 7186 (2015).
14. Alon, U. *An Introduction to Systems Biology: Design Principles of Biological Circuits* (CRC Press, 2006).
15. Berlow, E. L. et al. Simple prediction of interaction strengths in complex food webs. *Proc. Natl Acad. Sci. USA* **106**, 187–191 (2009).
16. Holland, J. N., DeAngelis, D. L. & Bronstein, J. L. Population dynamics and mutualism: functional responses of benefits and costs. *Am. Nat.* **159**, 231–244 (2002).
17. Pastor-Satorras, R. & Vespignani, A. Epidemic spreading in scale-free networks. *Phys. Rev. Lett.* **86**, 3200 (2001).
18. Dunne, J. A., Williams, R. J. & Martinez, N. D. Network structure and biodiversity loss in food webs: robustness increases with connectance. *Ecol. Lett.* **5**, 558–567 (2002).
19. Wilhelm, T., Behre, J. & Schuster, S. Analysis of structural robustness of metabolic networks. *Syst. Biol.* **1**, 114–120 (2004).
20. McCulloch, M., Falter, J., Trotter, J. & Montagna, P. Coral resilience to ocean acidification and global warming through pH up-regulation. *Nature Clim. Change* **2**, 623–627 (2012).
21. Hui, C. Carrying capacity, population equilibrium, and environment's maximal load. *Ecol. Model.* **192**, 317–320 (2006).
22. Allee, W. C. et al. *Principles of Animal Ecology* Edn 1 (WB Saunders, 1949).
23. Interaction Web Database http://www.nceas.ucsb.edu/interactionweb/resources.html#plant_ant (accessed 30 September 2010).
24. Balaji, S., Madan Babu, M., Iyer, L., Luscombe, N. & Aravind, L. Principles of combinatorial regulation in the transcriptional regulatory network of yeast. *J. Mol. Biol.* **360**, 213–227 (2006).
25. Gama-Castro, S. et al. Regulondb (version 6.0): gene regulation model of *Escherichia coli* k-12 beyond transcription, active (experimental) annotated promoters and txpresso navigation. *Nucleic Acids Res.* **36**, D120–D124 (2008).
26. Nepusz, T. & Vicsek, T. Controlling edge dynamics in complex networks. *Nature Phys.* **8**, 568–573 (2012).
27. Cornelius, S. P., Kath, W. L. & Motter, A. E. Realistic control of network dynamics. *Nature Commun.* **4**, 1942 (2013).
28. Majdandzic, A. et al. Spontaneous recovery in dynamical networks. *Nature Phys.* **10**, 34–38 (2013).
29. Helbing, D. & Vicsek, T. Optimal self-organization. *New J. Phys.* **1**, 13 (1999).
30. Cohen, R., Erez, K., Ben-Avraham, D. & Havlin, S. Breakdown of the internet under intentional attack. *Phys. Rev. Lett.* **86**, 3682–3685 (2001).

Supplementary Information is available in the online version of the paper.

Acknowledgements We thank A. Mohan, S. E. Flynn and A. R. Ganguly for discussions. This work was supported by an Army Research Laboratories Network Science Collaborative Technology Alliance grant (ARL NS-CTA W911NF-09-2-0053), by The John Templeton Foundation: Mathematical and Physical Sciences (grant number PFI-777), by The Defense Threat Reduction Agency (basic research grant number HDTRA1-10-1-0100) and by the European Commission (grant numbers FP7317532 (MULTIPLEX) and 641191 (CIMPLEX)).

Author Contributions All authors designed and did the research. J.G. and B.B. did the analytical calculations. J.G. analysed the empirical data and did the numerical calculations. A.-L.B. and B.B. were the lead writers of the manuscript.

Author Information All code for the reproduction of the reported results can be downloaded from <https://github.com/jianxiao/NuRsE>. Reprints and permissions information is available at www.nature.com/reprints. The authors declare no competing financial interests. Readers are welcome to comment on the online version of the paper. Correspondence and requests for materials should be addressed to A.-L.B. (alb@neu.edu).

CORRECTIONS & AMENDMENTS

ERRATUM

doi:10.1038/nature18019

Universal resilience patterns in complex networks

Jianxi Gao, Baruch Barzel & Albert-László Barabási

Nature **530**, 307–312 (2016); doi:10.1038/nature16948

In the last sentence of page 310 of this Letter, the parameter h should equal 2, rather than 1. In addition, after equation (4), the text should have stated ' $A_{ij} > 0$ ' and 'positive interactions', to read "...the weighted connectivity matrix $A_{ij} > 0$ captures the positive interactions between the nodes.". These errors have been corrected online.

CORRECTIONS & AMENDMENTS

CORRECTION

<https://doi.org/10.1038/s41586-019-1091-9>

Author Correction: Universal resilience patterns in complex networks

Jianxi Gao, Baruch Barzel & Albert-László Barabási

Correction to: *Nature* <https://www.nature.com/articles/nature16948>, published online 17 February 2016.

In this Letter, in Fig. 3c and f the *Saccharomyces cerevisiae* and *Escherichia coli* networks were subject to both weight loss and node deletion, a combination of two types of perturbation, as opposed to weight loss only (as the labelling incorrectly indicated). The collapse in Fig. 3h was also obtained from this combined perturbation, and therefore the results displayed in Fig. 3h remain fully consistent with the theoretical framework presented in this Letter. Figure 1 to this Amendment shows the corrected Fig. 3c, f and h, in which Fig. 3c and f have been generated with weight-loss perturbations only, as originally reported, together with the originally published panels, for completeness and transparency. The codes used to generate the original and the corrected Fig. 3 are available at <https://github.com/jianxigao/NuRsE>. We thank Travis A. Gibson for alerting us to this error. The original Letter has not been corrected.

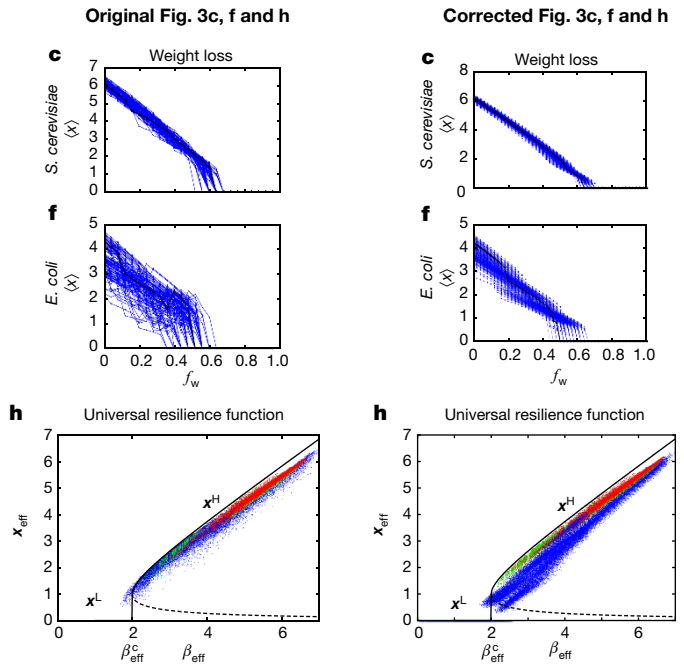


Fig. 1 | This figure shows the originally published Fig. 3c, f and h and the corrected Fig. 3c, f and h.